

Exchange flow through an opening

Echange de fluide à travers une ouverture

DAVID Z. ZHU, *Associate Professor, Department of Civil and Environmental Engineering, University of Alberta, Edmonton, AB, T6G 2G7, CANADA. Tel: (780) 492-5813; Fax: (780) 492-0249, E-mail: dzhu@civil.ualberta.ca*

HESHAM FOULI, *Graduate student, Department of Civil and Environmental Engineering, University of Alberta, Edmonton, AB, T6G 2G7, CANADA. E-mail: hfouli@ualberta.ca*

YAW A. OKYERE, *Graduate student, Department of Civil and Environmental Engineering, University of Alberta, Edmonton, AB, T6G 2G7, CANADA.*

ABSTRACT

This paper presents a theoretical and experimental study of the exchange of fluids of different densities through an opening. Three types of openings are examined: a bottom opening (the opening is at the bottom of a gate), a middle opening (in the middle) and a window opening (the opening is in the middle but does not extend across the width). Simultaneous measurements of velocity field and interface position were obtained using flow visualization and image processing techniques. Experimental results confirm the predictions of the internal hydraulic theory that there are two internal hydraulic controls in the flow through bottom openings, but one control in the middle and window opening experiments. The neglect of non-hydrostatic forces and interfacial mixing in the theory, however, results in a significant underestimate of the exchange rate by more than 50 % in the middle and window opening experiments. The fluctuations in the interface position were caused by Kelvin-Helmholtz instabilities as well as basin-scale internal seiche, and the transition of internally supercritical flow to subcritical flow was caused by the mixing generated by these instabilities.

RÉSUMÉ

Cet article présente une étude théorique et expérimentale de l'échange de fluides de densités différentes à travers une ouverture. Trois types d'ouvertures sont examinés : une ouverture au fond (l'ouverture est située à la base d'une vanne), une ouverture médiane (au milieu), et une fenêtre (l'ouverture est au milieu mais n'occupe pas toute la largeur). Des mesures simultanées de champ de vitesse et de position d'interface ont été faites avec des techniques de visualisation d'écoulement et de traitement d'image. Les résultats expérimentaux confirment les prédictions théoriques de l'hydraulique interne, à savoir qu'il y a deux contrôles hydrauliques internes pour l'écoulement à travers les ouvertures de fond, mais un seul contrôle pour l'ouverture médiane et la fenêtre. Cependant, le fait de négliger dans la théorie les forces non hydrostatiques et le mélange à l'interface conduit à sous-estimer le taux d'échange de plus de 50% dans les cas d'ouverture médiane et en fenêtre. Les fluctuations de l'interface étaient dues à des instabilités de Kelvin-Helmoltz, ainsi qu'à une seiche à l'échelle du bassin, et le passage torrentiel fluvial de l'écoulement interne était causé par le mélange dû à ces instabilités.

Keywords: Exchange flows, internal hydraulics, hydraulic control, opening, non-hydrostatic effects, interfacial instability, mixing.

1. Introduction

When two bodies of fluids of slightly different densities are connected by a channel, fluids start to exchange. Such exchange flows are common in nature; for example, the exchange of more saline Mediterranean Sea water with less saline Atlantic Ocean water through the Strait of Gibraltar (Armi & Farmer, 1988), the exchange flow through the Bosphorus (Oguz *et al.*, 1990), and the summertime exchange of warmer heavily polluted Hamilton Harbor water with cooler (more dense) Lake Ontario water through the Burlington ship canal (Hamblin & Lawrence, 1990). Two-layer exchange flows are commonly modeled as homogeneous layers of inviscid fluid with negligibly small vertical velocities. Consequently, the pressure distribution can be considered hydrostatic, and the hydraulic (or shallow water) equations can be applied to each layer. The extension of the hydraulic equations to two-layer flows is called the internal hydraulics; see for example, Armi (1986), Wood & Lai (1972). Previous studies on exchange flows have mostly focused on exchange flows through a channel where the change of channel geometry is gradual and the effect of non-hydrostatic forces can be neglected (Armi & Farmer,

1986). For such flows, Zhu (2002) developed a control curve approach to study exchange flows through complex geometry. Non-hydrostatic forces, however, could be important even for channels having smooth topography (Zhu & Lawrence 1998, 2000). Zhu & Lawrence (2000) showed that neglecting non-hydrostatic forces results in underestimating the flow rate even for exchange flows over a smooth topography.

Exchange flows through an opening are also common in nature. Examples of such flows include the exchange of cold and warm air through doorways and windows (Dalziel & Lane-Serff, 1991), the exchange of warm and cold water through a slot opening (Adams & Cosler, 1988) and in reservoir selective withdrawal (Harleman & Elder, 1965). Dalziel & Lane-Serff (1991) noted that the basic features of doorway exchange flow could be described by the internal hydraulics. By approximating the rapidly varying doorway geometry as a slowly varying channel, they neglected the effects of non-hydrostatic forces and assumed that the flow is critical at the doorways and window opening. Similarly, Adams & Cosler (1988) did not consider the effects of non-hydrostatic forces.

Given that exchange flows through a sharp opening tend to have

Revision received November 19, 2001. Open for discussion till October 31, 2002.

strong streamline curvature, as is evident in single-layer flow over a sharp-crested weir, it is questionable that the non-hydrostatic forces caused by streamline curvature can be neglected. Detailed experimental studies on these flows are needed in order to understand the hydraulics of the flows and to evaluate the effects of non-hydrostatic effects. Previous experimental studies by Adams & Cosler (1988) and Dalziel & Lane-Serff (1991) do not provide simultaneous measurements of the interface position and the flow rate, thus not sufficient for such study.

The objective of this study is to seek a better understanding of the hydraulics of exchange flows through various types of openings, and to examine the applicability of the internal hydraulics to these flows. Laboratory experiments were conducted and detailed flow measurements were taken using flow visualization and image processing techniques. The paper is structured as follows: Section 2 reviews the internal hydraulics and discusses the control mechanisms of exchange flows through various types of openings. Section 3 presents the experimental setup and apparatus. Sections 4 and 5 discuss experimental results and the comparison with theoretical predictions for exchange flows through an opening at the bottom and in the middle, respectively. Some interesting observations of the flow, such as interfacial instabilities and mixing mechanisms, are also discussed. The paper is concluded in Section 6.

2. Hydraulics of Exchange Flow Through an Opening

In this section, we will first briefly review the internal hydraulics for inviscid flow with a hydrostatic pressure distribution. We will then apply it to study exchange flows through various types of openings. To facilitate our discussion, we start by considering exchange flows through a combination of a bottom sill and a surface inverted sill in a rectangular channel, which connects two large reservoirs containing fluids of slightly different densities (Fig. 1). Provided the sills have gentle curvature, the pressure distribution will remain close to hydrostatic and thus the internal hydraulics is valid. The streamline curvature, however, increases when the sills become shorter. When the sills become infinitely short, this case becomes the flow through a sharp opening. It is the intent of this study to examine whether the internal hydraulics is still valid for such flows.

In the present study we focus on flows with small density difference, i.e. $\varepsilon = (\rho_2 - \rho_1)/\rho_2 \ll 1$, where ρ_1 and ρ_2 are the densities of the upper and lower layer, respectively. For such flows, the slope of the free surface is negligibly small, commonly referred to as the 'rigid lid' or horizontal free surface approximation. Thus the elevation of the free surface

$$H = y_1 + y_2 + h_1 + h_2 \quad (1)$$

remains a constant, where y_1 and y_2 are the thickness of the upper and lower layer, and h_1 and h_2 are the thickness of the surface and bottom sill, respectively.

For shallow water flows, it is customary to assume that the pressure is hydrostatic, and that the horizontal velocity is uniform across depth in each layer. For steady, inviscid and irrotational

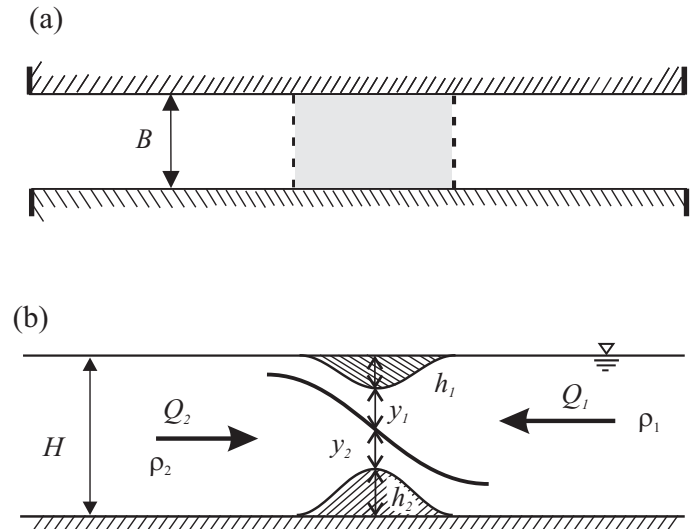


Fig. 1. Illustrating diagram showing two-layer exchange flows through a channel with sills. (a) Plan view, (b) side view.

flows, the energy head (or Bernoulli constant) E_i for layer i , ($i = 1, 2$), is conserved in the absence of hydraulic jumps or flow separation. Thus the internal energy E ,

$$E \equiv (E_2 - E_1)/(\rho_2 - \rho_1)g = y_2 + h_2 + (U_2^2 - U_1^2)/2g' \quad (2)$$

is also conserved along the channel. Here g is the gravitational acceleration, $g' = \varepsilon g$ is the reduced gravitational acceleration, and U is the mean horizontal velocity.

The conservation of the internal energy E together with the rigid-lid free surface condition (Eq. 1) gives the slope of the interface position,

$$d(y_2 + h_2)/dx = \{F_1^2 h_{1x} - F_2^2 h_{2x} - (F_1^2 y_1 - F_2^2 y_2) b_x / b\} / (1 - G^2) \quad (3)$$

where $F_i^2 = U_i^2 / g' y_i$ is the densimetric Froude number for layer i , $G^2 = F_1^2 + F_2^2$ is the composite (or internal) Froude number, and b is the width of the channel. Subscript x indicates the differentiation with respect to x .

The locations where $G = 1$ are known as internal hydraulic controls and the flow is said to be internally critical at these locations. The composite Froude number G acts in a similar manner to the Froude number F for single-layer flows with the flow being internally supercritical (or subcritical) when $G > 1$ (or $G < 1$). In subcritical flows, small interfacial disturbances can propagate towards both upstream and downstream, while they propagate only downstream in supercritical flows.

Possible locations of controls can be determined using Eq. (3) from the requirement that the numerator be zero. For flows where sills are separated from channel contractions, controls can only occur at sill crests or channel narrowest points. For each control, we can develop a relationship between the internal energy E and the flow rate Q using $G = 1$ together with Eq. (2). Such a relation, or a control curve (Zhu, 2002), represents all possible solutions of the flow with the control. Control curve technique is a power-

ful tool in analyzing two-layer flows and will be used in the following study.

It is convenient to normalize the flow variables with respect to the vertical scale H , the lateral scale B , the velocity scale $(g'H)^{1/2}$, and the flow rate scale $HB(g'H)^{1/2}$. The characteristic time scale, T , is equal to the total volume of water in the tank, AH , where A is the surface area of the tank, divided by the flow rate scale, *i.e.*, $T = (A/B)/(g'H)^{1/2}$. With these scalings, we obtain the following set of dimensionless variables:

$$y_i^* = y_i/H; \quad h_i^* = h_i/H; \quad b^* = b/B; \quad E^* = E/H; \quad (4)$$

$$U_i^* = U_i/(g'H)^{1/2}; \quad Q_i^* = Q_i/(HB(g'H)^{1/2}); \quad t^* = t/T$$

where the parameters with an asterisk are dimensionless. For the remainder of this paper, dimensionless parameters will be used and the asterisks will be dropped.

2.1. Flow Through a Bottom Opening

Without the bottom sill, *i.e.* $h_2 = 0$ but $h_1 \neq 0$ in Fig. 1, the flow exchanges through an opening at the bottom that extends across the channel width B (Fig. 2a). Note that when the sill becomes very short, this case is similar to flow through a sharp opening. Here the sill crest control will also be called the opening control. The exchange flow through a bottom opening tends to be critical at the opening. A control curve for the opening control (or crest control) (Zhu, 2002) is plotted in Fig. 3, where $h_1 = 0.43$ and $h_2 = 0$ are used to simulate the conditions in Exp. B2 (discussed below). For the exchange flow shown in Fig. 1, a possible second control is located at the channel exit. The control curve for the exit control is also shown in Fig. 3. Clearly, with both the opening control and the exit control, the rate of exchange is determined by both controls and is obtained at the intersection point of the two control curves.

With two controls, the exchange flow is subcritical in the region bounded by the controls, but supercritical immediately outside. Given that interfacial disturbances cannot propagate against supercritical flows, the influence of the reservoirs is blocked by the controls. Exchange flow with two controls is called the maxi-

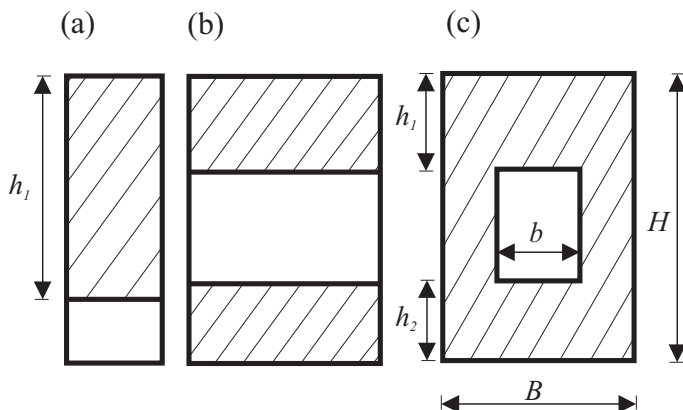


Fig. 2. Types of openings: (a) bottom opening, (b) middle opening, (c) window opening.

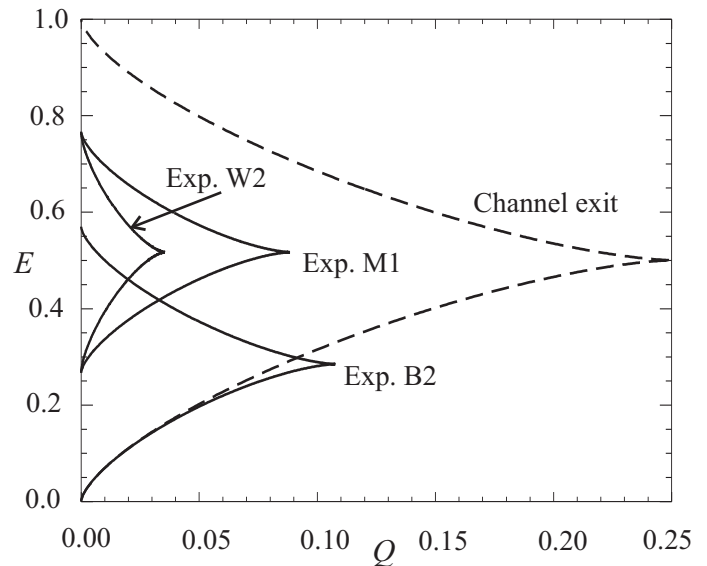


Fig. 3. Control curves showing solutions to the exchange flow through bottom, middle and window openings.

— control curve for the opening control.
 - - - control curve for the exit control.

mal exchange, as it gives the maximal flow rate for a given channel geometry and density difference. The maximal exchange flow is steady before one of the controls is flooded. When the exit control is lost due to the rise of the interface level in the right hand reservoir, the flow will then be subcritical all the way to that reservoir. Exchange flow with one control only is called the submaximal exchange, and is influenced by the variation in the reservoir condition. Submaximal exchange is determined by the remaining control together with the internal energy E specified by the reservoir condition.

2.2. Flow Through Middle and Window Openings

A middle opening (Fig. 2b) can be modeled by having finite values of h_1 and h_2 . The case where an opening does not extend across the channel width (Fig. 2c) is called a window opening and is considered separately. The control curve for a middle opening is plotted in Fig. 3 with $h_1 = 0.23$ and $h_2 = 0.27$ to simulate Exp. M1. Noticeably different from a bottom opening, the control curve for a middle opening no longer intersects with the exit control curve, indicating that the flow cannot satisfy both controls. The flow is now controlled by the opening alone. The maximal flow rate $Q_{max} = \frac{1}{4} B (1 - h_1 - h_2)^{3/2}$ is obtained when $E = \frac{1}{2} (1 - h_1 - h_2)$ or $y_1 = y_2$ at the opening (see Zhu (2002) for details on control curves). The flow is critical at the opening and supercritical away from it. The single control in this flow is due to the increase in the bottom elevation at the opening such that the influence of the exit is blocked by the supercritical flow leaving the opening.

The case of a window opening (Fig. 2c) is similar to a middle opening, except for the additional lateral contraction. This lateral contraction will act to decrease the flow rate given $b < B$. The control curve for a window opening with $b = 0.4$ but the same h_1 and h_2 as in Exp. M1 is also plotted in Fig. 3. Similar to the mid-

dle opening, the exchange flow through a window opening is controlled solely by the opening where the flow is also symmetric with $y_1 = y_2$ at the opening.

3. Experiments

Experiments of exchange flows through an opening were conducted in a water tank of 245 cm long, 123.5 cm wide and 35 cm high (Fig. 4). The tank was divided into two reservoirs, which were connected by a rectangular channel of 150 cm long. The density difference was obtained by dissolving a known amount of salt (NaCl) into the left hand reservoir. Three types of openings were studied: a bottom opening, a middle opening and a window opening (Fig. 2). In experiments with a bottom opening, the height of the opening was varied (Exp. B1 – B4). In the middle opening experiments, the height of the opening was varied (Exp. M1 – M2), while the width of the opening was varied in the window opening experiments (Exp. W1 – W2). An additional experiment was conducted to study the effect of barotropic forcing by pumping fluid from one side of the reservoir to the other (Exp. F1). Detailed conditions for these experiments are summarized in Table 1.

Table 1. Table of experiments

Exp.	Opening	g' (cm/ s ²)	h_1/H	h_2/H	b/B opening width	Q^* flow rate	B channel width (cm)	L length scale (cm)	T time scale (s)
B1	Bottom	2.74	0.27	0	1	0.133	10	90	327
B2	Bottom	2.72	0.43	0	1	0.095	10	90	335
B3	Bottom	2.73	0.63	0	1	0.053	10	90	334
B4	Bottom	2.74	0.73	0	1	0.030	10	90	334
F1**	Bottom	2.72	0.67	0	1	0.087	10	90	335
M1	Middle	2.50	0.23	0.27	1	0.139	20	75	175
M2	Middle	3.19	0.40	0.27	1	0.080	20	75	155
W1	Window	2.50	0.23	0.27	0.7	0.101	20	75	175
W2	Window	2.50	0.23	0.27	0.4	0.071	20	75	175

Water depth $H = 30$ cm in all experiments, except in Exp. F1 where $H = 22.5$ cm.

* Flow rate was measured during the steady period of the experiments.

** Fluid was pumped from the right reservoir to the left, and the channel bed was raised by 7.5 cm.

A plate with an opening was fixed in the channel. The plate was located in the middle of the channel for the middle and window opening experiments. Thus the distance between the plate and the right-hand exit of the channel, L , is 75 cm. In the bottom opening experiments, the plate was moved towards left to give a larger L of 90 cm. Before the experiments, a barrier was inserted in the channel to separate the two reservoirs. Salt was added into the left hand reservoir, as well as sodium fluorescing dye to indicate the lower layer. Tiny neutrally buoyant tracer particles (Pliolite VT-L) were added into both reservoirs.

After removing the barrier, an exchange flow developed. Experiments were illuminated from above using a thin sheet of light generated by two 500-Watt halogen bulbs. Images of tracer particles and interface position were recorded separately using Sony Hi8 video cameras. The velocity field halfway between the opening and the channel right-hand exit was obtained by tracking the

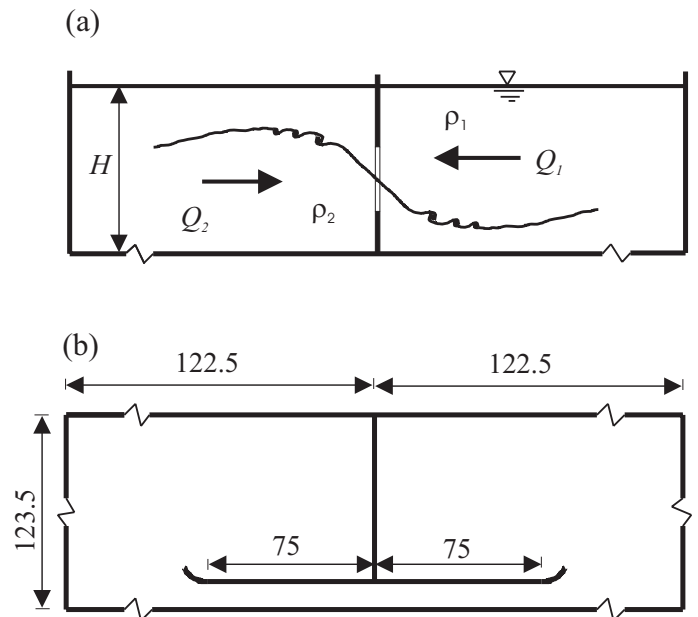


Fig. 4. Experimental setup: (a) side view, and (b) plan view. All dimensions are in centimeters

movements of tracer particles using a maximal cross-correlation technique (Steven & Coates, 1994). The location of the density interface was determined from the maximal gradient of light intensity between the transparent upper layer and the dyed lower layer. Using particles and dyes, simultaneous measurements of velocity field and interface positions were obtained.

Errors in the measurements of flow velocity field and flow rate are dependent on the resolution of the video images. Images of 640 x 480 pixels covered a flow area of 40 cm (horizontal) by 30 cm (vertical), giving a pixel resolution of 0.06 cm. In determining the velocity field the time interval between two images was chosen to ensure that particles had an average travel distance of approximately 10 pixels (0.6 cm), resulting in an error of approximately 10 % in velocity due to pixel resolution. This error was reduced to about 3 % by averaging 10 neighboring velocity profiles. Flow rate was then obtained by integrating velocity profiles over the depth. The errors in locating the free surface and the bottom positions (about 1 pixel) further increased the error in flow rate. This error was reduced by additional averaging over four flow rates obtained from four pairs of images taken within a second. We estimate a possible error of about 5 % in flow rate measurements.

Errors in the measurements of the interface position are mainly due to the relatively low resolution of the video images. In bottom opening experiments, the interface position from the opening to the channel right-hand exit is of interest. Images of 640 x 480 pixels covered a channel length of 120 cm. This gave a pixel resolution of about 0.2 cm. Errors of 1 – 2 pixels in the determination of the interface position correspond to relative errors of 1 – 3 %. In the middle and window opening experiments, the images centered around the opening and covered a channel length of 60 cm, yielding a pixel resolution of about 0.1 cm. This allows a more accurate measurement of the interface position. In all measurements, various averaging was performed on the data.

4. Exchange Flow Through a Bottom Opening

We start this section by discussing the evolution of the flow regimes. The experimental measurements are then compared with the predictions of the internal hydraulics. This is followed by the results of exchange flow with barotropic forcing.

4.1 Evolution of the Mean Flow

The exchange flow started when the barrier separating the two reservoirs was removed. After an initial unsteady period, the hydraulic control at the opening was first established. At a later time, the exit control was also established. With two controls the flow was steady maximal exchange (Fig. 5a). During the experiment, the interface level in the right-hand reservoir rose continuously as a result of the accumulation of the denser water. When it exceeded a certain level, the exit control was then flooded, and the flow was submaximal exchange (Fig. 5b). The flow rate in this submaximal exchange decreased continuously given the rise in the interface level in the right-hand reservoir. The following study focuses on the steady maximal flow regime.

The evolution of the flow regime is illustrated using the measurement of the flow rate in Exp. B2, as shown in Fig. 6. The steady maximal exchange started at $t \approx 0.3$ and lasted until $t \approx 1.3$. After that the flow rate decreased due to the loss of the exit control. During the steady maximal exchange, the flow rate remained constant. The small variation in the measurements is probably due to experimental errors. Errors in Exp. B2 have a standard deviation of about 2 %, consistent with our analysis of about 5 % error in flow rate measurement. Note that in this experiment, the water level is the same in both reservoirs, such that the flow in the up-

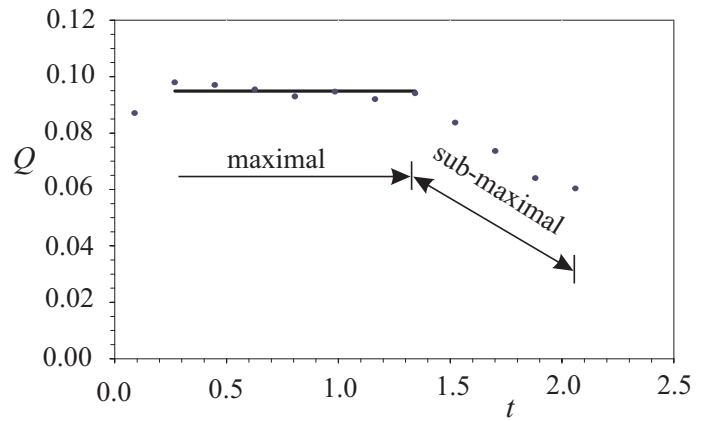


Fig. 6. Measurements of the flow rate with time in Exp. B2. — mean flow rate.

per layer must be balanced by the flow in the lower layer, i.e. $Q_1 = Q_2$.

4.2 Hydraulics of the Flow

Along-channel variation of the interface position was measured between the opening and the right-hand exit of the channel. A mean interface position was obtained by averaging out the interface fluctuations due to shear-generated instabilities, and is plotted in Fig. 7(a) for Exp. B2 during its maximal exchange regime. The upper layer converged when the flow moved from right to left. A circulating surface eddy formed upstream of the opening. This eddy effectively reduced the thickness of the upper layer, and was considered in determining the layer thickness. Unlike the interface position, the determination of the eddy size proves to be more difficult and has some uncertainty.

Using the measured flowrate and interface position, the along-channel variation of the composite Froude number G is obtained for Exp. B2 (Fig. 7b). It is obvious that this flow has two controls located at the opening and at the exit, as predicted by the internal hydraulics. Between the two controls, the flow is subcritical. Note that accurate determination of G at the opening is difficult as a small error in locating the horizontal position would result in a significant change in G . At the exit, the end effect also affects the G value. The G values at the opening and at the exit were found to be in the range of 0.9 – 1.2 for Exp. B1 – B4. Recalling that the flow rate and the layer thickness could have a possible error of 5 % and 3 %, respectively, G could have a possible error of about 12 %. Thus the above measurements of G at the opening and the exit compare well with the prediction of the internal hydraulics. Variation of the internal energy E is plotted in Fig. 7(c). Instead of remaining constant as predicted by the internal hydraulics, E varies as a result of friction and non-hydrostatic forces. The friction at the interface, sidewalls and the bottom causes E_1 to increase and E_2 to decrease in the positive x -direction. Thus E , which is determined by subtracting E_1 from E_2 (Eq. 2), also decreases in the x -direction. The effect of friction is clearly seen in Fig. 7(c) where E decreases with x . Around the gate where streamline curvature is significant, the non-hydrostatic forces cause E to increase significantly with x . The internal energy E

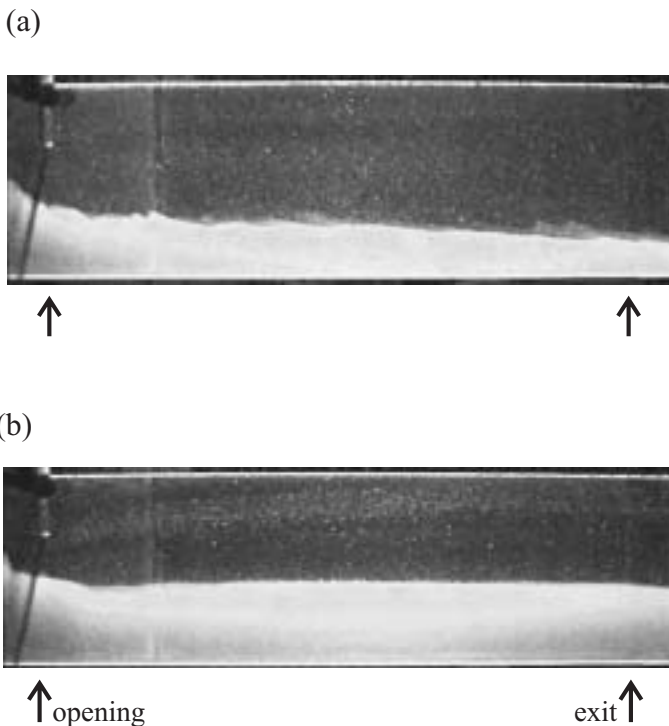


Fig. 5. Images showing the flow regimes in Exp. B1: (a) maximal exchange, (b) sub-maximal exchange.

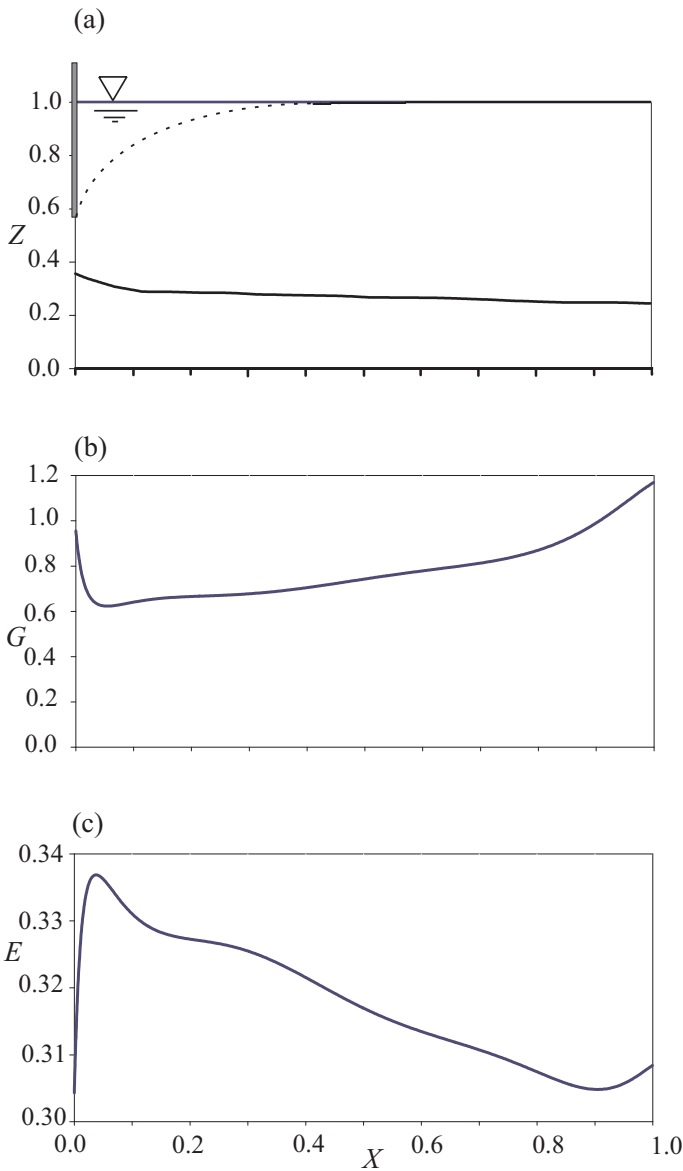


Fig. 7. Measurements of the along-channel variations of (a) the mean interface position, (b) the composite Froude number G , and (c) the internal energy in Exp. B2.

also increases at the channel exit but to a lesser extent. The non-hydrostatic effects are much smaller in the middle of the channel where friction is dominant. It is interesting to note that the effects of non-hydrostatic forces and friction tend to cancel each other in Exp. B2, and the internal energy E is very much the same at the gate and at the exit.

Measurements of the flow rate in Exp. B1 – B4 are compared with the predictions of the internal hydraulics for inviscid and hydrostatic flow in Fig. 8. With the controls at the gate and the channel exit, the internal hydraulics predicts the flow rate very well. Zhu & Lawrence (2000) showed that friction reduces the flow rate while non-hydrostatic forces tend to increase the flow rate. As these effects cancel each other as shown in Exp. B2, neglecting friction and non-hydrostatic forces does not cause major error in flowrate prediction. Note, however, that friction is more important in longer channels while non-hydrostatic forces depend on local streamline curvatures. In addition, accurate prediction of

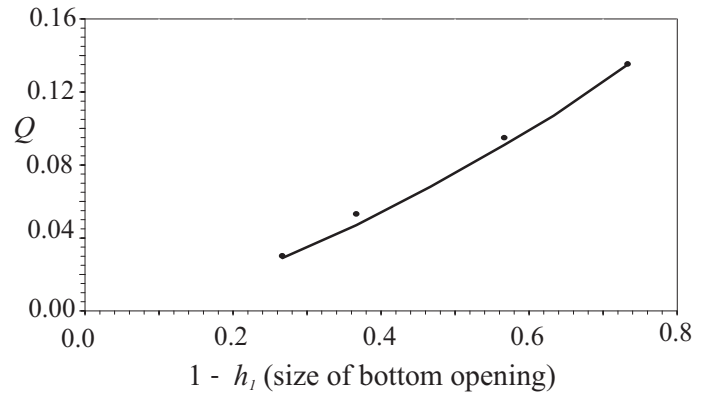


Fig. 8. Comparison of measured and predicted flow rates for exchange flows through a bottom opening of different sizes (Exp. B1 – B4). * measurements, — prediction.

the interface position requires that both effects be considered (Zhu & Lawrence, 2000).

4.3 Exchange Flow with Barotropic Forcing

One experiment (Exp. F1) was conducted to study the effect of barotropic forcing on exchange flows. In the experiment, the denser fluid was pumped from the right to the left reservoir to maintain a net flow between the two layers, and the channel bottom was raised by 7.5 cm over the bottom of the reservoir in order to maintain the exit control for a longer period. When the net flow is strong enough it can arrest the upper layer and leave only the lower layer moving. Figure 9 shows the arrested flow observed in Exp. F1 where the upper layer was stagnant and only the lower layer was moving. At the interface of the two-layers, a special type of interfacial instability, namely, Holmboe instability (Zhu & Lawrence, 2001) is observed. Since the flow was almost parallel in a major section of the channel, this arrested flow provides an ideal condition to study Holmboe instability.

Given that only the lower layer was active, G was calculated based on the lower layer only. At the opening, G was 0.77 in Exp. F1, smaller than the measurements in the non-forcing cases. Harleman & Elder (1965) also reported smaller values with G ranging from 0.17 to 0.88 in their arrested flows. It is to be noted that there is some uncertainty in computing the G value at the opening. In Exp. F1, the contribution of the upper layer in G was neglected given the negligibly small flow rate in the upper layer. However, since the upper layer is significantly thinner (< 0.5 cm) than the lower layer (7.0 cm), an upper layer flow rate of only

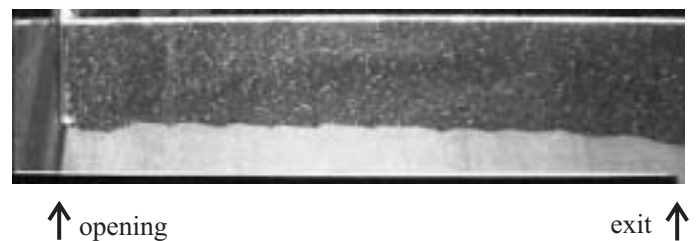


Fig. 9. Image showing an exchange flow with barotropic forcing in Exp. F1 where the upper layer is arrested.

2 % of the lower layer will yield the same Froude number in the upper layer as in the lower layer. The significant contribution in G by such a small flow rate in the upper layer makes the accurate determination of G difficult. This might be the reason that the reported G values vary significantly in the literature.

At the channel exit, G was measured at 1.82. This large G value is due to the fact that the channel bottom was raised. Thus after the exit, the lower layer falls over as in single-layer flow. Assuming that the brink depth is 0.715 of the critical depth as in single-layer flow (Henderson, 1966), this would yield a value of 1.65 for G at the exit, which is close to our measurement.

5. Exchange Flow Through Middle and Window Openings

In the middle and window opening experiments, the control at the opening was established shortly after the start of the experiments, and the flow became steady. Eventually the opening control was lost and the flow became unsteady. In this study, we will focus on the steady exchange. The hydraulics of the flows will first be examined and the measurements of flow rate will be compared with theoretical predictions. The results of the mean interface position and its fluctuations will then be discussed. Finally the transition from the supercritical to subcritical flow will be studied.

5.1. Flow Controls and Flow Rate

Images of the flow through a middle opening (Exp. M1) and a window opening (Exp. W1) are shown in Fig. 10. The interface fluctuated due to significant interfacial instabilities generated by the strong velocity gradient. In order to obtain a mean position of the interface, a time series of the interface position at the opening was obtained during the steady maximal regime in Fig. 11(a) for Exp. M1. The mean interface position was at 0.511, which is about the mid-depth of the opening of 0.517. The mean interface position was also measured to be at the mid-depth of the opening in Exp. W1.

For exchange flow through middle and window openings, the internal hydraulics predicts a maximal exchange rate of $Q_{max} = \frac{1}{4} b (1 - h_1 - h_2)^{3/2}$ based on $G = 1$ and $y_1 = y_2$ at the opening. The measurement of the interface position confirms the prediction that $y_1 = y_2$ at the opening. The flow rate measurements, however, are significantly larger than the predictions (Fig. 12). They are 57% and 69% larger than the predictions for the larger and smaller middle openings, respectively; and they are 63% and 100% larger than the predictions for the larger and smaller window openings, respectively. These flow rates were measured halfway between the opening and the channel right hand exit. At this location, the flow was parallel thus allowing an accurate measurement of the flow rate.

The above results are significantly different from the bottom opening experiments where the measured flow rates compared well with the predictions. The reason for this difference needs further study, but we hypothesize that it is due to the non-hydrostatic forces as well as the entrainment at the interface of the two layers. Zhu & Lawrence (2000) reported that the inclusion of non-hydrostatic forces results in an increase of 15% in flow rate

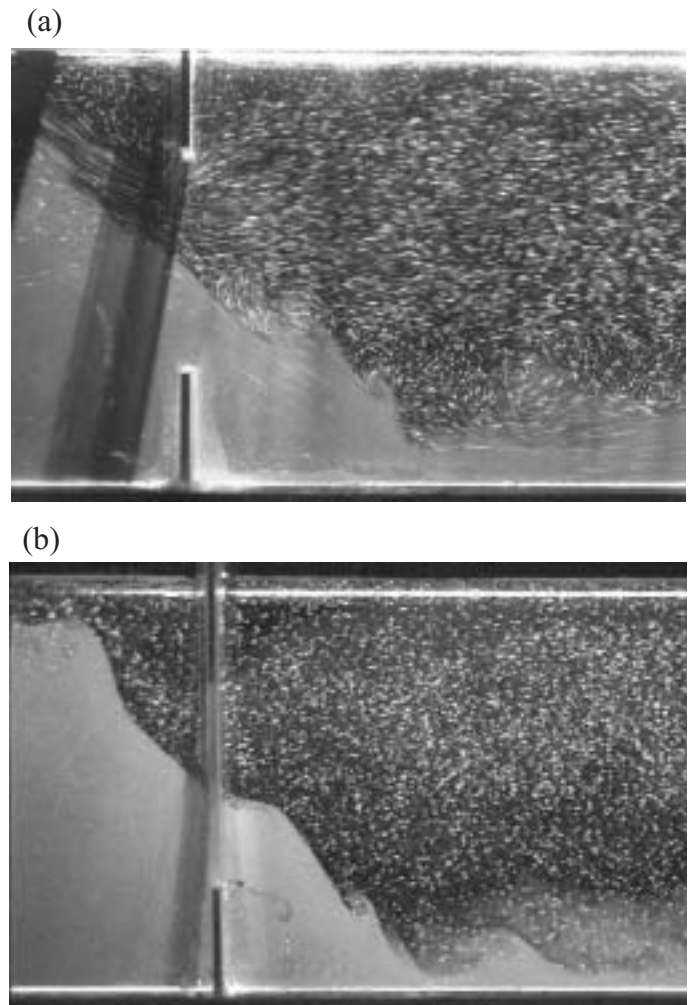


Fig. 10. Images showing the exchange flow through (a) a middle opening (Exp. M1), and (b) a window opening (Exp. W2).

in their flow over a smooth sill. In the bottom opening experiments, the friction between the two controls reduces the flow rate, and the effects of friction and non-hydrostatic forces cancel each other. Thus neglecting both effects in the prediction does not cause significant error. In the middle and window opening experiments, the flow is controlled at the opening only. Friction has minimal effect, whereas non-hydrostatic forces become even more important given strong streamline curvature. Neglecting non-hydrostatic forces results in significantly underestimating the flow rate. The fact that the error in the flow rate increases with decreasing opening size seems to further confirm the importance of non-hydrostatic forces.

Passing through the opening, the fast-moving lower layer entrains the fluid from the upper layer. This entrainment thus results in an increased flow rate in both the upper and lower layer. The rate of entrainment has been studied for some simple flows such as density currents (see, for example, Alavian et al, 1992). Recent study by Morin et al. (2002) showed that the flow rate is increased by 20% for the exchange flow over a smooth sill of 10 cm high and 50 cm long due to the interfacial entrainment. Detailed study is needed in order to quantify the amount of the flow rate increase due to the interfacial entrainment for the flows studied here.

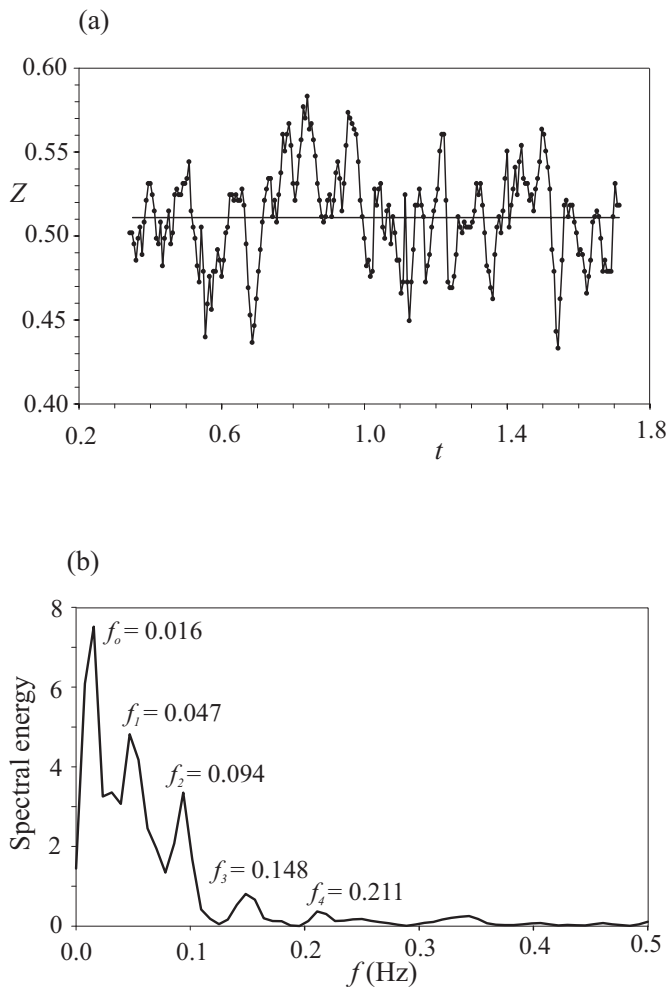


Fig. 11. (a) Time series of the interface position at the opening in Exp. M1 (the time-averaged value is also indicated), and (b) its spectrum.

5.2. Interface Position

The interface of the exchange flows is subject to the fluctuations generated by interfacial instabilities as well as basin-scale oscillations (i.e. internal seiche). The processes responsible for the inter-

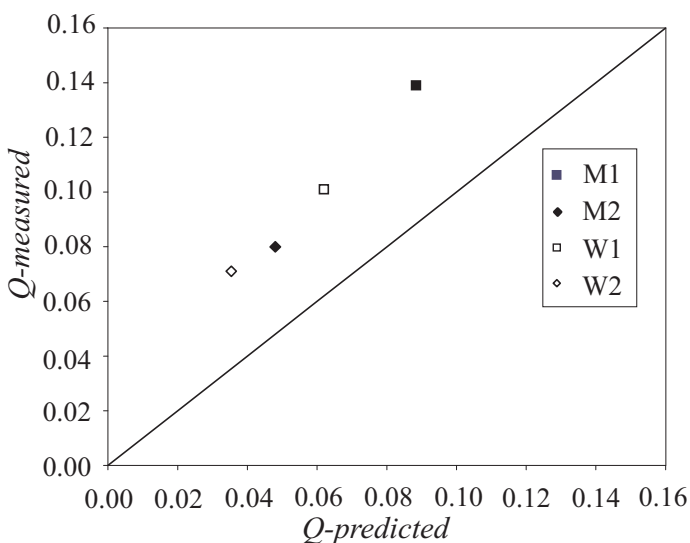


Fig. 12. Comparison of measured and predicted flow rates for the exchange flow through middle and window openings.

face fluctuations will be first studied, followed by an examination of the mean position of the interface.

The time series of the interface position measured at the opening in Exp. M1 (Fig. 11a) was analyzed and its spectrum is shown in Fig. 11(b). Five spectral peaks can be identified. The most dominant peak has the lowest frequency f_0 of 0.016 Hz, corresponding to an oscillating period of 62.5 seconds. This low frequency oscillation is believed to be associated with the basin internal seiche. A quick estimate of the seiche period can be obtained by assuming the reservoir is a closed two-dimensional basin with a length $L_b = 123$ cm. The propagating speed of the interfacial wave is given by $C_1 = \sqrt{g' y_1 y_2 / (y_1 + y_2)}$ (Zhu & Lawrence, 2000). Assuming the interface is at the mid-depth of the reservoir, i.e., $y_1 = y_2 = 15$ cm, the fundamental mode of the internal seiche has a period of $T_0 = 2L_b/C_1 = 56.8$ seconds. This compares well with the measurement of 62.5 seconds. Note that the actual seiche period will be affected by some factors that are not considered in this simple model: the effect of the connecting channel and the fact that the basin is close to rectangular (i.e. three dimensional). Nevertheless these effects appear to be of secondary importance.

The next two spectral peaks have frequencies of $f_1 = 0.047$ Hz and $f_2 = 0.094$ Hz (or $T_1 = 21.3$ s and $T_2 = 10.6$ s). These frequencies are believed to be associated with the Kelvin-Helmholtz (K-H) instabilities generated at the interface. Detailed examination of the video images indeed revealed that the dominant periods of the K-H instabilities generated close to the opening are either 10 s or 20 s. Other spectral peaks have frequencies of $f_3 = 0.148$ Hz and $f_4 = 0.211$ Hz. It is clear that $f_2 (\approx 2.0f_1)$, $f_3 (\approx 3.1f_1)$, and $f_4 (\approx 4.5f_1)$ are the first, second and third harmonics of the base frequency f_1 . The existence of the third and fourth harmonics in interfacial instabilities has not been reported in the literature. Further study on these instabilities requires a detailed measurement of the flow field at the opening and is beyond the scope of this study.

The mean position of the interface will now be examined. The shape of the lower layer in the middle and window opening experiments is similar to a nappe in a single-layer flows over a sharp-crested weir, while the upper layer is like an inverted nappe (Fig. 10a). The mean position of the lower layer, also called 'nappe' here, was obtained by averaging its position over duration of 2 minutes at one second interval. Figure 13 shows the mean profile of the nappes in the middle and window opening experiments. The surface re-circulation zone is also plotted in Fig. 13. It is of interest to compare the trajectory of these nappes to that in a single-layer flow with its surface position at the weir the same as the interface position. Notice that the exchange flow here is significantly different from a single-layer flow. In particular, the flow at the opening has a much larger vertical acceleration. Figure 13 clearly shows that the horizontal momentum of the nappe was killed much quicker and the nappe hit the bed closer to the opening in the exchange flows compared to a one-layer flow. This is because in the exchange flows, hydrostatic pressure increases down the nappe due to the increase in the upper layer thickness. In addition, there is significant friction along the nappe. These are significantly different from a single-layer flow where the pressure at both the upper and lower nappe remains atmo-

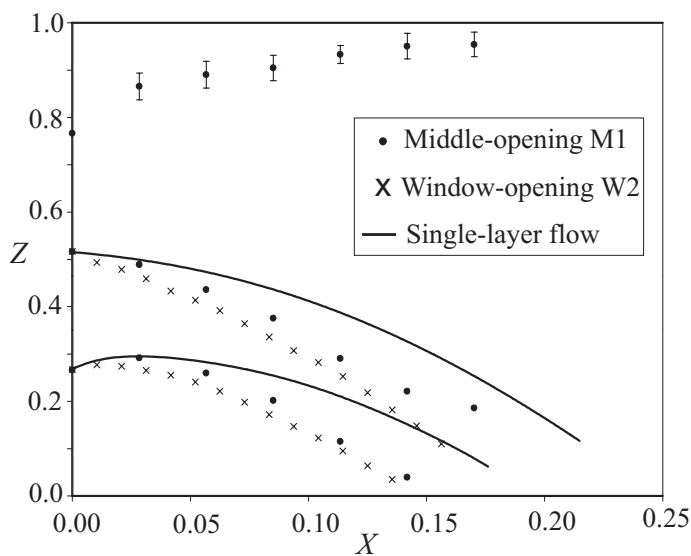


Fig. 13. Mean position of the lower layer in Exp. M1 and Exp. W2, compared with the nappe profile in single-layer flow over a sharp-crested weir.

spheric and the friction at the air-water surface is negligibly small. Furthermore, the significant vertical velocity in the exchange flows also helped to reduce the horizontal trajectory of the nappe. In the window experiments, the lateral expansion in the lower layer along the nappe further helped to reduce the horizontal trajectory of the nappe.

An interesting observation in Exp. W2 is that the lighter fluid was continuously being fed into the underneath of the lower nappe. This was seen as a pocket of clear fluid underneath the dyed lower layer (Fig. 10). Recall in single-layer flow over a weir, aeration is required under the lower nappe to maintain the pressure atmospheric. In window opening experiments, the under-pressure below the lower nappe was caused by the entrainment of the nappe, which resulted in the lighter fluid being fed there.

5.3. Transition to Subcritical Flow

The flow leaving the opening was internally supercritical in the experiments with middle and window openings. It is usually believed that this supercritical flow will go through an internal hydraulic jump to subcritical as prescribed by the downstream flow condition in the reservoirs. However, internal hydraulic jumps were not observed in any of the above experiments. Instead, the transition to the subcritical flow was completed through the expansion of the thin lower layer by the mixing caused by large K-H instabilities as is evident in Fig. 10. In the transition region, a mixed layer of intermediate density between the upper and lower layers was observed. This mixing zone eventually disappeared and the flow became two-layered again downstream.

Earlier studies have examined the velocity profile of a single-layer flow over a sharp-crested weir (Montes, 1998). Here we will examine the variation of G assuming that the flow rate is constant along the channel and velocity is uniform across the depth. Based on an averaged layer thickness, the variation of G downstream of the opening in Exp. M1 is shown in Fig. 14. The flow is internally supercritical at the opening with $G \approx 1.5$. This G value increases

to about 3.1 at $x \approx 0.3$ where the transition to subcritical flow starts. Though the lower layer thins continuously, G actually decreases at $x \approx 0.1$ as the upper layer thickens quickly due to the surface re-circulation eddy and its contribution in G reduces. The flow starts to approach uniform at $x \approx 0.5$ where $G \approx 1.3$, and becomes internally subcritical with $G \approx 0.8$ at $x \approx 0.65$. Note that the variation in the flow rate along the channel due to the entrainment and the uncertainty in determining the layer thickness can result in significant error in the estimates of G values, especially where mixing is appreciable.

6. Summary and Conclusions

Exchange flows through bottom, middle and window openings were studied theoretically and experimentally. Simultaneous measurements of the velocity field and the interface position were obtained using particle tracking and imaging processing techniques. Utilizing control curves, the internal hydraulic theory predicts the existence of two controls in the exchange flow through bottom openings. In the exchange flows through middle and window openings, the influence of the exit is blocked by the supercritical flow away from the opening. These flows thus have only one control located at the opening, with the interface located at the center of the opening. These predictions are confirmed in the experiments.

The internal hydraulic theory, however, could significantly underpredict the rate of exchange as it neglects the effects of friction, non-hydrostatic forces and interfacial entrainment. Inclusion of non-hydrostatic forces increases the prediction of the flow rate, whereas friction reduces the flow rate. In the bottom opening experiments, the friction between the two controls cancels out the effects of non-hydrostatic forces, and the predictions of the flow rate compare well with the measurements. In the middle and window opening experiments, on the other hand, the flow is controlled at the opening only. Thus friction has minimal effect in the flow rate, whereas non-hydrostatic forces become even more important given strong streamline curvature. Neglecting non-hydrostatic forces results in underestimating the flow rate. The effect of streamline curvature together with the interfacial entrainment causes an increase in flow rate by 50 – 100 % over the theoretical predictions.

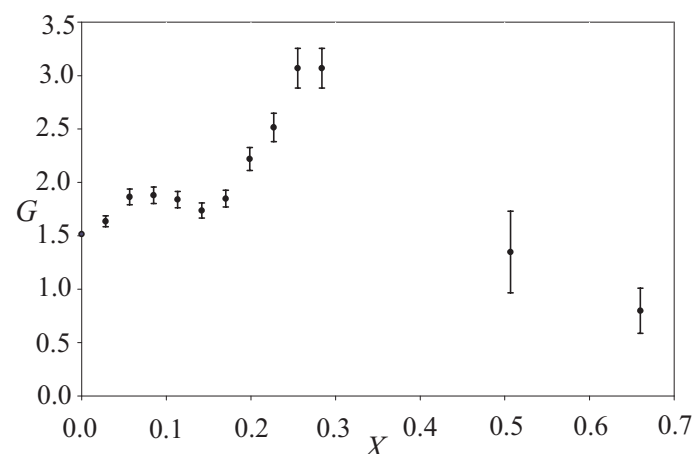


Fig. 14. Variation of G along the channel in Exp. M1 with error bars.

In the middle and window opening experiments, the interface of the two layers fluctuates due to the Kelvin-Helmholtz instabilities generated at the interface, as well as the low frequency basin-scale internal seiche. The observation of several modes of higher frequency oscillations is unexpected. These are believed to be higher harmonics of the fundamental mode of K-H instabilities. The mean position of the lower layer was measured and its horizontal trajectory is found to be much shorter compared to that in a single-layer flow. The transition of this supercritical flow to subcritical was completed through the expansion of the thin lower layer by the mixing caused by large K-H instabilities.

Exchange flow through a bottom opening with the upper layer arrested was also examined. A smaller G value was reported at the opening, consistent with earlier studies. This is due to the neglect of the upper layer in calculating G . Given the upper layer is significantly thinner than the lower layer at the opening, a very small flow rate in the upper layer could have significant contribution in G , thus there is some uncertainty in computing the G value at the opening.

References

- ADAMS, E.E. and COSLER, D.J. (1988). Density exchange flow through a slotted curtain. *J. Hydr. Res.* 26, 261-273.
- ALAVIAN, V., JIRKA, G.H., DENTON, R.A., JOHNSON, M.C. and STEFAN, H.G. (1992). Density currents entering lakes and reservoirs. *J. Hydr. Eng.*, ASCE, 118(11), 1464-1489.
- ARMI, L. (1986). The hydraulics of two flowing layers with different densities. *J. Fluid Mech.*, 163, 27-58
- ARMI, L. and FARMER, D.M. (1986). Maximum two layer exchange through a contraction with Barotropic net flow. *J. Fluid Mech.*, 164, 27-51.
- ARMI, L. and FARMER, D.M. (1988). The flow of Mediterranean water through the Strait of Gibraltar. *Progress in Oceanography*, 21, 1-105.
- DALZIEL, S.B. and LANE-SERFF, G.F. (1991). The hydraulics of doorway exchange flows. *Building and Environment*, 26, 121-135.
- HAMBLIN, P.F. and LAWRENCE, G.A. (1990). Exchange flows between Hamilton Harbor and Lake Ontario. *Proc. of 1990 Annual Conf. of Canadian Society for Civil Eng.*, V: 140-148.
- HARLEMAN, D.R.F. and ELDER, R.A. (1965). Withdrawal from two-layer stratified flows. *J. Hydr. Div.*, ASCE, 91(4), 43-58.
- HENDERSON, F.M. (1966). *Open Channel Flow*. Macmillan Press.
- MONTES, S. (1998). *Hydraulics of Open Channel Flow*. ASCE Press.
- MORIN, V.M., ZHU, D.Z. and LOEWEN, M.R. (2002). Instability and entrainment in exchange flow over a smooth sill. *J. Hydr. Eng.*, ASCE, submitted.
- OGUZ, T., OZSOY, E., LATIF, M.A., SUR, H.I. and UNLUATA, U. (1990). Modeling of hydraulically controlled exchange flow in the Bosphorus Strait. *J. Physical Oceanography*, 20, 945-965.
- STEVEN, C. and COATES, M. (1994). Applications of maximized cross-correlation technique for resolving velocity fields in laboratory experiments. *J. Hydr. Res.*, 32, 195-212.
- WOOD, I.R. and LAI, K.K. (1972). Flow of layered fluid over broad crested weir. *J. Hydr. Div.* ASCE, 98, 87-104.
- ZHU, D.Z. (2002). Control curves for two-layer flows. *J. Hydr. Eng.*, ASCE, 128(1), 113-116.
- ZHU, D.Z. and LAWRENCE, G.A. (1998). Non-hydrostatic effects in layered shallow water flows, *J. Fluid Mech.*, 355, 1-16.
- ZHU, D.Z. and LAWRENCE, G.A. (2000). Hydraulics of exchange flows. *J. Hydr. Eng.*, ASCE, 126(12), 921-928.
- ZHU, D.Z. and LAWRENCE, G.A. (2001). Holmboe's instability in exchange flows. *J. Fluid Mech.*, 429, 391-409.